SCIENTIFIC REPORTS

OPEN

SUBJECT AREAS:
BIOMEDICAL ENGINEERING
PRE-CLINICAL STUDIES

Received
2 January 2014

Accepted
28 March 2014

Published
15 April 2014

Correspondence and requests for materials should be addressed to B.H.Y. (baohong@uta.edu)

* These authors contributed equally to this work.

† Current address: Department of Bioengineering, The Pennsylvania State University, University Park, PA 16802, USA.

High resolution imaging beyond the acoustic diffraction limit in deep tissue *via* ultrasound-switchable NIR fluorescence

Yanbo Pei[1,2]*, Ming-Yuan Wei[1,2]*, Bingbing Cheng[1,2], Yuan Liu[1,2], Zhiwei Xie[1,2]†, Kytai Nguyen[1,2] & Baohong Yuan[1,2]

[1]Department of Bioengineering, The University of Texas at Arlington, Arlington, TX 76019, USA, [2]Joint Biomedical Engineering Program, The University of Texas at Arlington and The University of Texas Southwestern Medical Center at Dallas, TX 75390, USA.

Fluorescence imaging in deep tissue with high spatial resolution is highly desirable because it can provide details about tissue's structural, functional, and molecular information. Unfortunately, current fluorescence imaging techniques are limited either in penetration depth (microscopy) or spatial resolution (diffuse light based imaging) as a result of strong light scattering in deep tissue. To overcome this limitation, we developed an ultrasound-switchable fluorescence (USF) imaging technique whereby ultrasound was used to switch on/off the emission of near infrared (NIR) fluorophores. We synthesized and characterized unique NIR USF contrast agents. The excellent switching properties of these agents, combined with the sensitive USF imaging system developed in this study, enabled us to image fluorescent targets in deep tissue with spatial resolution beyond the acoustic diffraction limit.

Fluorescence microscopy has been widely used in biological and medical studies because it can provide subcellular images with structural, functional, and molecular information[1,2]. In addition to cellular or subcellular information at the superficial tissue level, micro-information, such as microcirculation in sub-centimeter- or centimeter-deep tissue, is also important for studying both healthy and diseased tissues[1–4]. Unfortunately, microscopy is limited to imaging superficial tissues (submillimeter in depth) because tissue scatters light so strongly that the light cannot be optically focused in deep tissue[1,2]. Instead of focusing light, fluorescence diffuse optical tomography (FDOT) detects highly scattered light and thus can image centimeter-deep tissues but suffers from poor spatial resolution (millimeters)[5–8]. As a result, the micro-information is lost in FDOT. To reveal such essential information, high resolution fluorescence imaging in deep tissue is highly desirable.

To achieve this aim, several techniques recently have been proposed and demonstrated, such as multispectral optoacoustic tomography[9], ultrasound-modulated fluorescence[10,11] or luminescence[12], ultrasound-induced temperature-controlled fluorescence[13–15], and time-reversed ultrasonically encoded optical focusing (TRUE)[16–20]. These techniques take advantage of the large penetration depth of diffused light (meaning highly scattered light) and tightly focused ultrasound to acquire fluorescence images in deep tissues ($\gg$1 mm). Compared with FDOT, the resolution of these techniques depends on ultrasound frequency and is dramatically improved without sacrificing the imaging depth. Although significant progress has been made, the acoustic diffraction limit, a new barrier, essentially hinders further improvement in the resolution.

To break the acoustic diffraction limit, spatially or temporally applied multiple sound–light interactions based on TRUE have been adopted to focus the light into a region smaller than the focal size of the adopted ultrasound wave[19,20]. Thus, the spatial resolution can be improved beyond the acoustic diffraction limit. While TRUE-based techniques have shown promising results in static samples, significant challenges remain for imaging dynamic samples because the time reversal of light (one of the key techniques in TRUE-based methods) in deep living tissue is intrinsically vulnerable to dynamic processes, such as blood flow[19,21].

Recently, we proposed a concept of ultrasound-switchable fluorescence that has the potential to break the acoustic diffraction limit based on its unique switching features[15]. Two major components are included in USF imaging: (1) USF contrast agents and (2) an ultrasound-controlled optical imaging system. First, USF contrast agents are used to label the tissue. Then, the labeled tissue is scanned by the system through an area of interest to image the distribution of the USF contrast agents. Unlike TRUE-based methods, USF does not rely on optical time

reversal and therefore is not susceptible to tissue's dynamic processes. The principle of USF imaging is based on the unique switching properties of the contrast agent whose fluorescence can be switched on and off *via* a focused ultrasound wave. To apply this technique for imaging subcentimeter- or centimeter-deep biological tissue beyond the acoustic diffraction limit, one major challenge is the need to develop near infrared (NIR) USF contrast agents that have outstanding switching properties, such as a large ON-to-OFF ratio in fluorescence intensity (I_{ON}/I_{OFF}), a sharp transition between OFF and ON states (T_{BW}), and an adjustable switching threshold (T_{th}). NIR light can efficiently minimize tissue absorption and therefore can penetrate centimeter-deep tissue. It excites minimal tissue autofluorescence and thus can avoid background noise[22]. A large ratio of I_{ON}/I_{OFF} is essential for suppressing the background fluorescence noise generated by fluorophores in the OFF state (so-called non–100% off fluorescence) and enhancing the signal produced by ultrasonically switched-on fluorophores. Unfortunately, such an NIR USF contrast agent has not been developed to date. The challenge in the imaging system is how to efficiently differentiate the USF signals from the noise. In the current study, we developed a family of NIR USF contrast agents that have a large ratio of I_{ON}/I_{OFF} (~3–9), which has not been achieved by other contrast agents (~1.8)[14]. We also developed a sensitive USF imaging system. Combining the unique contrast agents and the imaging system, we demonstrated that the NIR USF technique can break the acoustic diffraction limit for high-resolution imaging in deep tissue.

Results

NIR USF contrast agents. We synthesized a family of USF contrast agents by encapsulating an environment-sensitive NIR dye of indocyanine green (ICG) into thermo-sensitive nanoparticles (NPs). **Fig. 1A** schematically shows the USF concept of the synthesized NPs. When the environment's temperature is below a threshold (the lower critical solution temperature (LCST) of the NPs), the NPs are hydrophilic and absorb a dramatic amount of water. Therefore, their size is relatively large[23]. ICG molecules fluoresce weakly in water-rich microenvironments because water provides a polar and nonviscous solvent microenvironment, which can increase the nonradiative decay rate of the excited fluorophores. When the temperature increases above the threshold (LCST), the NPs experience a phase transition from hydrophilic to hydrophobic. Thus, the water molecules are dramatically expelled from the NPs, and the NPs significantly shrink. Accordingly, the ICG molecules inside the NPs are exposed to a polymer-rich microenvironment, which has a relatively lower polarity and higher viscosity compared with the water-rich microenvironment. This type of microenvironment can suppress the nonradiative decay rate of the excited fluorophores[24,25], and therefore the fluorescence intensity from the ICG increases dramatically. This phase transition caused by the environment's temperature crossing LCST is reversible. A high intensity focused ultrasound (HIFU) transducer can be used to control the temperature in its focal volume and then locally switch on/off the contrast agents[15].

The NPs are made of thermo-sensitive polymers of either poly (N-isopropylacrylamide) (PNIPAM) or its copolymer with acrylamide (AAm) or N-tert-butylacrylamide (TBAm). For the chemical structures, see **Fig. S1** in *Supplementary Information*. Copolymerizing an appropriate amount of AAm or TBAm can increase or decrease the LCST (and therefore the switching threshold) of the copolymer compared with the pure PNIPAM polymer. ICG is a commonly used NIR dye that has a peak excitation at 780 nm and a peak emission at 830 nm[26]. Our data show that ICG is more sensitive to the change of the solvent's polarity than to that of the solvent's viscosity (see **Fig. S2**). The size of the NPs was found to be between 70 and 150 nm *via* dynamic light scattering and transmission electron microscopy (see **Fig. S3**). The chemical structures of the dye can be found in **Fig. S1**, and the synthesis protocols are provided in the *Methods*.

Four USF contrast agents were synthesized, including (1) ICG-encapsulated P(NIPAM-TBAm 185:15) NPs, (2) ICG-encapsulated PNIPAM NPs, (3) ICG-encapsulated P(NIPAM-AAm 90:10) NPs, and (4) ICG-encapsulated P(NIPAM-AAm 86:14) NPs. The ratio in each NP refers to the molar ratio between the monomer of NIPAM and the monomer of TBAm or AAm. The composition of these NPs was confirmed by Fourier transform infrared results (see **Fig. S4**). The switching curve of each synthesized NP is shown in **Fig. 1B**, in which the fluorescence intensity is plotted as a function of the sample temperature. The sharp switching features clearly can be seen for all the four USF NPs with different switching thresholds (LCSTs: 28, 31, 37, and 41°C, respectively; see the figure caption for details). The I_{ON}/I_{OFF} can reach 2.9, 3.3, 9.1, and 9.1, respectively, corresponding to the four LCSTs, which are 1.6–5.1 times higher than that of other contrast agents[14]. This is mainly attributed to the extremely high temperature sensitivity of PNIPAM. To verify whether the NPs can be repeatedly used, **Fig. 1C** shows the data measured from one of the samples of ICG-encapsulated P(NIPAM-AAm 90:10) NPs at low (25°C) and high (44°C) temperatures. The fluorescence intensity can be repeatedly switched between the two temperatures. The results suggest that the ICG molecules are not likely to be released in a short period because of their relatively larger molecular weight (774.96 g mol^{-1}) compared with that of a water molecule (18 g mol^{-1})[23].

Sample configuration. A small silicone tube (with a mean inner diameter of 0.69 mm) was filled with the aqueous solution of the ICG-encapsulated PNIPAM NPs (LCST = 31°C) and embedded into a piece of porcine muscle tissue to simulate a blood vessel as a target for USF imaging. **Fig. 2A** shows the configuration of the tissue sample, the tube, the excitation light, the fluorescence collection fiber, and the high intensity focused ultrasound (HIFU) transducer. The porcine tissue has a thickness of ~8 mm (z) and a width of 20 mm (x). The tube was inserted into the tissue along the y direction. The distance from the tube center to the top surface of the tissue is ~4 mm. A fiber bundle with a diameter of ~3 mm (Edmund Optics NT39-366, New Jersey) was used to deliver the excitation light from a laser to the bottom of the tissue to excite the HIFU switched-on fluorophores. The second fiber bundle (Edmund Optics NT42-345) was placed on the top of the tissue to collect USF photons. A 2.5 MHz HIFU transducer (H-108, Sonic Concepts, Washington; active diameter: 60 mm; focal length: 50 mm) was positioned at the bottom of the tissue and focused on the tube region. To efficiently transmit the acoustic energy into the tissue, the HIFU transducer, the bottom surface of the tissue sample, and the fiber bundle for delivering the excitation light were submerged into water. For imaging the tube two dimensionally, the HIFU transducer was scanned on the x-y plane.

USF imaging system. The setup of the USF imaging system is shown in **Fig. 2B**. The system mainly consists of four subsystems: (1) an optical system, (2) an ultrasonic system, (3) a temperature measurement system, and (4) an electronic control system. The optical system includes the delivery of the excitation light and the collection of the emission light. The excitation light is generated from an 808 nm laser and is delivered to the bottom of the sample tissue *via* the fiber bundle. Although the laser is operated in a continuous wave mode (continuously illuminates once turned on), the time delivering the light to the sample and the illumination duration are controlled by using a fast mechanical shutter (UNIBITZ LS3T2, New York) that is triggered by a pulse delay generator (PDG). The collected fluorescence photons *via* the second fiber bundle are delivered to a set of emission filters and then received by a photomultiplier tube (PMT). The carefully designed combination of the four emission filters can maximally reject the excitation photons and pass the emission fluorescence photons. The signal after the PMT is further amplified and

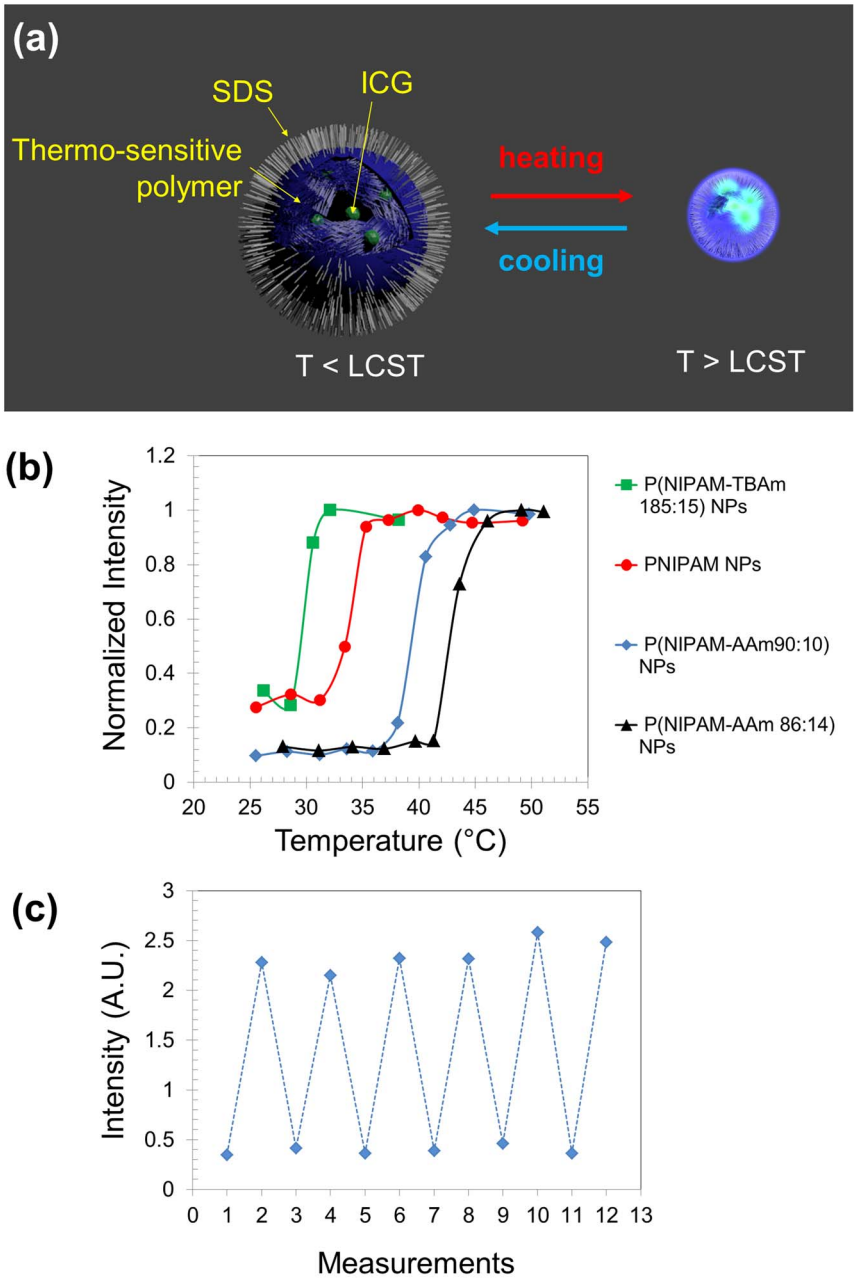

Figure 1 | (a) Illustration of ICG-encapsulated thermosensitive nanoparticles (NPs) as a USF contrast agent. LCST: lower critical solution temperature. The internal structure of the particles was shown by cutting off one section of the particle. (b) Normalized fluorescence intensity of the four USF contrast agents as a function of the sample temperature. (c) Repeatable switching of the fluorescence intensity of ICG-encapsulated P(NIPAM-AAm 90:10) NPs (as one example). The low and high temperature points are 25 and 44°C, respectively.

then acquired by an oscilloscope. The ultrasonic system consists of the HIFU transducer and the driving components, including an impedance matching network (NWM), a radio-frequency (RF) power amplifier, and a function generator (FG). The temperature at the HIFU focus is measured by a micron-sized thermocouple *via* an amplifier and the second oscilloscope. The entire system is controlled by the PDG, including the firing of the HIFU heating pulse, the firing of the excitation light pulse, and the data acquisition of the oscilloscope. The time sequence of these processes is plotted in **Fig. 2C**. In this study, the ultrasonic exposure time is 300 ms, determined by the width of the gating pulse from the PDG. During the ultrasonic exposure period, the tissue temperature at the HIFU focus rises. After the exposure, the temperature reduces as a result of thermal diffusion. The excitation light illuminates the tissue for 2 ms right before the end of the ultrasonic exposure. At the same time, the fluorescence signal is acquired by the oscilloscope, which is triggered by a pulse from the PDG. The HIFU transducer is scanned by a two-dimensional translation stage. The details about the system can be found in *Methods*.

High resolution USF images. Fig. 3A shows a USF image of the tube on the x-y plane. The two vertical dashed lines indicate the locations of the inner edges of the tube. The full-width-at-half-maximum (FWHM) and the full-width-at-one-eighth-of-the-maximum (FWEM) of the USF image profile along the x direction at each y location were calculated. The averaged FWHM and FWEM at different y locations were 0.48 ± 0.13 mm and 0.68 ± 0.19 mm, respectively. Although the FWHM (0.48 mm) is narrower than the inner diameter of the tube, the FWEM (0.69 mm) is very close to the tube's inner diameter (0.69 mm). This is understandable because

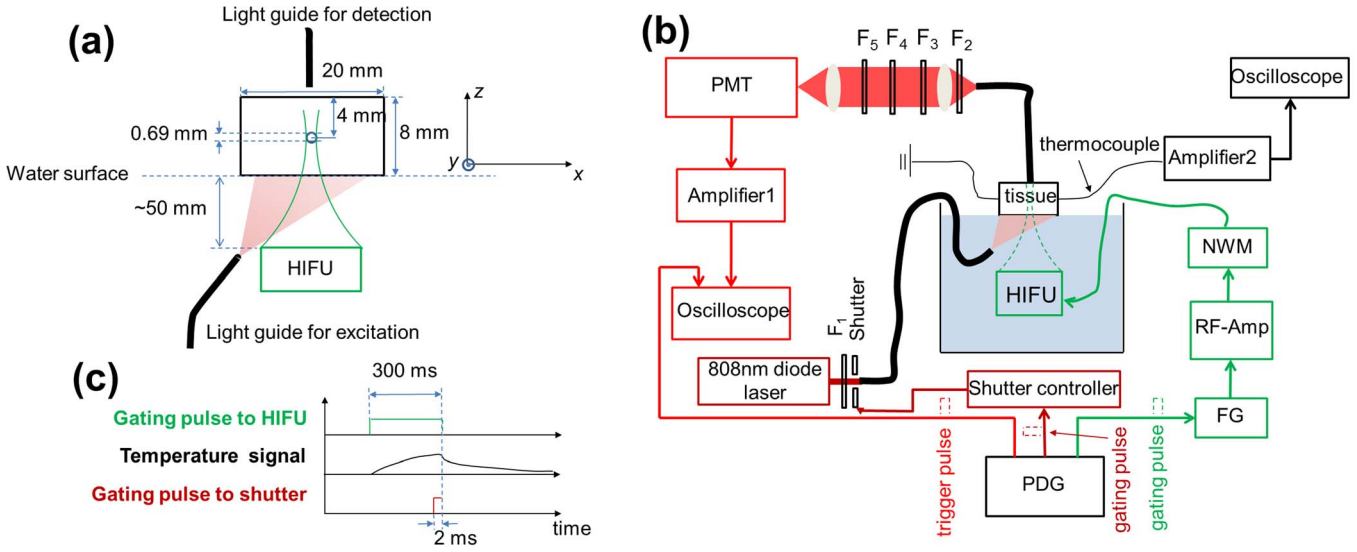

Figure 2 | (a) The sample configuration, including the tissue, the tube, the excitation and emission fiber bundles, and the HIFU transducer. (b) The schematic diagram of the USF imaging system. PDG: pulse delay generator; FG: function generator; RF-Amp: radio-frequency power amplifier; MNW: matching network; HIFU: high intensity focused ultrasound; Amplifier 1: low noise current preamplifier; PMT: photomultiplier tube; F1: excitation filter; F2–F5: emission filters; Amplifier 2: an amplifier circuit consisting mainly of a high-precision operational amplifier OPA2277. (c) The timing diagram showing the gating pulse to the HIFU transducer and the shutter. The gating pulse to the HIFU determined the heating period (300 ms in this study). During the heating period, the temperature in the focal volume increased continuously. At the final 2 ms of this duration, the shutter was opened to excite the fluorescence signal. At the same time, the oscilloscope was triggered for data acquisition.

the inner diameter is a parameter describing the full size of the tube. Therefore, the FWEM, instead of the FWHM, can be considered a parameter describing the full size of the USF image.

To compare the USF image with a pure ultrasound image, the same sample was scanned on the x-y plane using the same HIFU transducer *via* the commonly used pulse-and-echo method (see the details in *Methods*). At each x-y location, the reflected ultrasonic echo from the top inner boundary of the tube was recorded and used to generate the ultrasound image. The result is shown in **Fig. 3B**. Its averaged FWHM and FWEM are 0.76 ± 0.01 mm and 1.12 ± 0.02 mm, respectively, and both are larger than those of the USF image.

Fig. 3C and **Fig. 3D** shows the comparison among the profiles of USF, diffused fluorescence light, ultrasound, and temperature along the horizontal dashed line marked in **Fig. 3A**. The FWHM of the diffused fluorescence signal is 3.9 mm (see the black line with "x" in **Fig. 3C** and the details in *Methods* about how the signal was measured). It is significantly larger than the FWHM of the corresponding USF's profile (0.48 mm; see the blue solid line) and the tube's inner diameter (0.69 mm). This overestimation is commonly seen in FDOT, mainly because of the dramatic light scattering caused by the thick tissue. This result indicates that the USF has much higher resolution than does FDOT. The FWHMs of the temperature profile (0.66 mm; see the red line with squares in **Fig. 3D**) and the ultrasound profile (0.76 mm; see the black line in **Fig. 3D**) are also larger than that of the USF profile (0.54 mm; see the blue line with squares in **Fig. 3D**). These results indicate that the USF achieves the highest resolution among the techniques mentioned above.

Estimation of the FWHM of the point spread function. To estimate the FWHM of the point spread function of the USF imaging system, we adopted the following strategies. (1) A smaller tube (inner diameter: 0.31 mm) was also scanned. (2) Because further reducing the tube size was difficult and limited by the signal-to-noise, we mathematically de-convolved the tube profile data from the acquired USF profile data. The average FWHM of the estimated point spread functions of both the large and small tubes was 0.29 mm. For the ultrasound imaging system, if one assumes that

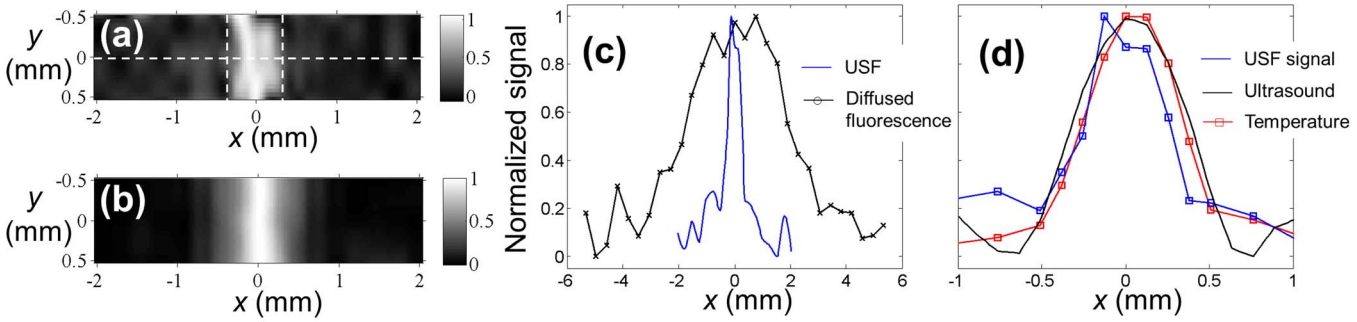

Figure 3 | (a) The USF image of the tube embedded into the porcine muscle tissue. ICG-encapsulated PNIPAM NPs were used as the contrast agents. The two dashed vertical lines represent the inner boundaries between the tube and USF contrast agents. (b) The diffraction-limited ultrasound image (C-mode) of the same tube in the tissue, obtained by raster scanning the same HIFU transducer on the x-y plane. (c) The profiles of the USF signal and the diffused fluorescence signal along the x axis at y = 0 (see the dashed horizontal line in **Fig. 3A**). (d) The profiles of the USF, ultrasound, and temperature signals along the x axis at y = 0. Both the USF and ultrasound image were normalized and interpolated based on a bicubic method[18].

the ultrasound speed in muscle is between 1,542 and 1,626 m/s, the FWHM of the diffraction-limited lateral focal size (equivalent to the FWHM of the lateral point spread function) of the adopted HIFU transducer (frequency = 2.5 MHz and f-number = 0.83) is theoretically between 0.512 and 0.54 mm. Therefore, the estimated size of the point spread function of the USF system is smaller than that of the ultrasound system. The above result clearly indicates that USF can achieve a resolution beyond the acoustic diffraction limit.

Discussion

The synthesized USF contrast agents in this study have the following advantages. First, they are NIR contrast agents and therefore can be used for deep-tissue imaging. Second, their ON-to-OFF ratios (I_{ON}/I_{OFF}) are a few times higher than those of the existing contrast agents. Third, the switching threshold (T_{th}) can be well controlled and therefore can be potentially used for *in vivo* animal studies in the future whereby the T_{th} should be slightly higher than body temperature (37°C). Fourth, the transition between on and off states is sharp (generally ~3–5°C). Such a narrow transition bandwidth (T_{BW}) is necessary for efficiently switching on/off fluorescence and avoids potential tissue thermal damage in animal studies. Fifth, the excellent switching repeatability of the developed USF contrast agents allows acquisition of multiple images at the same location for either improving signal-to-noise ratio (SNR) *via* averaging or monitoring tissue dynamic processes.

Generally, the USF signal is weak and may be contaminated with noise. This problem becomes even more severe when high resolution is desired. This is because the high resolution requires the small focal size and therefore the small amount of USF contrast agents in the focal volume can be switched on. Thus, the amount of the detectable USF photons (the desired signal) dramatically decreases as the resolution increases, while the amount of the noise photons remains stable because noise is not correlated with the focal size and the resolution (see the next paragraph). Accordingly, to successfully image the small tube in deep tissue, it is necessary to optimize the USF imaging system and use the NIR USF contrast agent with a large I_{ON}/I_{OFF}.

The PMT-received photons potentially consist of four components: (1) excitation photons from the laser due to the leakage of the emission filters, (2) tissue autofluorescence photons within the pass band of the emission filters, (3) photons emitted from the non–100% off USF contrast agents, and (4) USF photons. The first three components are the major noise sources. They can be generated from the entire tissue sample and are not correlated with the ultrasound focus. Therefore, they can be called global noise. The last component is the desired signal, which is uniquely related to the ultrasound focus. It can be called local signal. As the resolution increases, the SNR quickly reduces. Accordingly, minimizing the global noise and increasing the signal level become critical. In the current system, the laser leakage has been significantly suppressed by using the specially designed combination of the emission filters (see the details in *Methods*). The adoption of the NIR USF contrast agents dramatically avoids the autofluorescence noise. The large value of I_{ON}/I_{OFF} limits the noise generated from the non–100% off contrast agents and also improves the USF signal. Therefore, it is feasible to differentiate the local USF signal from the global noise by directly monitoring the fluorescence intensity change at different locations.

Two possible mechanisms may lead to breaking the acoustic diffraction for achieving high resolution—a nonlinear acoustic effect and a threshold effect—both of which have been discussed in our recent publications[15,27,28]. Briefly, when a nonlinear acoustic effect occurs, both lateral and axial focal sizes are dramatically reduced below the diffraction-limited size, which can improve the USF spatial resolution. Furthermore, because of the existence of a threshold to switch on fluorescence, USF contrast agents can be switched on only in a volume where the temperature is above the threshold. The size of this volume is usually smaller than the actual size of the ultrasound focal volume if one appropriately selects the threshold and ultrasound exposure power[15]. Thus, the spatial resolution of the USF technique can be further improved.

It is worth mentioning that the axial resolution of the USF is usually worse than the lateral axial if a single element HIFU transducer is used because the exposure time is at the level of hundreds of milliseconds (so called quasi continuous wave exposure mode). However, this problem can be overcome by using two confocal transducers with an angle of 90 degrees. The overlapped focal volume has a much more uniform size along the lateral and axial directions than has the focal volume of a single transducer. This has been demonstrated in the literature[29]. In addition, another important feature of USF is that it provides fluorescent contrast that is usually sensitive to both tissue structural and molecular information (if appropriately conjugating the USF agents with targeting moieties). When using contrast agents with different excitation and emission wavelengths, multiple types of molecules may be imaged via spectroscopic techniques, which is usually difficult for non-optical imaging techniques.

Lastly, thermal and non-thermal bio-effects caused by HIFU in the USF imaging technique may be a concern for future applications. Our studies show that the thermal damage can be completely ignored because of the very short HIFU exposure time (see the detailed discussion in the *Supplementary Information*). Mechanical damage is the major non-thermal bio-effect. The mechanical index (MI) adopted in this study was estimated to be ~2.5 and is slightly higher than the FDA-required MI < 1.9 for human in diagnostic ultrasound. However, it is worth pointing out that MI = 2.5 is not required and lower MI should also works for USF imaging. Quantitative investigation between the USF signal-to-noise ratio and MI is necessary in future. In addition, this value can be reduced by adopting several strategies that are discussed in the *Supplementary Information*.

In conclusion, we synthesized a family of NIR USF contrast agents based on ICG-encapsulated PNIPAM NPs. These NPs have excellent switching properties based on the fluorescence-intensity ratio between on and off states, the narrow transition bandwidth, the adjustable switching threshold, and the switching repeatability. The developed USF imaging system was optimized to clearly differentiate the USF photons from the background noise. When combining the contrast agents and the imaging system, we demonstrated that the USF imaging technique could break the acoustic diffraction limit for high-resolution imaging in deep tissue.

Methods

Materials. N-isopropylacrylamide (NIPAM), acrylamide (AAm), ammonium persulfate (APS), sodium dodecyl sulfate (SDS), N,N,N′,N′-tetramethyl ethylene diamine (TEMED), N,N′-methylenebisacrylamide (BIS), N-tert-butylacrylamide (TBAm), sodium ascorbate, and ICG were purchased from Sigma-Aldrich (St. Louis, MO, USA). All chemicals were used as purchased without further purification.

Synthesis protocols. The ICG-encapsulated PNIPAM NPs were used as one example to describe the protocol, and others are similar. ICG was added directly into the reaction solution prior to the polymerization and then loaded into the NPs, likely as a result of the ampliphic property of the ICG molecule itself. NIPAM (monomer, 0.6822 g), BIS (cross-linker, 0.0131 g), and SDS (surfactant, 0.0219 g) were dissolved with 50 mL de-ionized water in a 250 mL Schlenk tube, followed by purging with nitrogen for 10 minutes. ICG (fluorophore, 0.0034 g), APS (initiator, 0.039 g), and TEMED (accelerator, 51 μL) were added into the tube, which was vacuumed and then filled with nitrogen. The vacuuming/filling procedure was repeated three times to secure a nitrogen-protected environment inside the reaction tube. The reaction was conducted at room temperature for 4 hours and thereafter stopped by exposure to air when the valve was loosened. The sample was dialyzed against deionized water, using a 10-kDa molecular weight cutoff membrane for 3 days to remove extra surfactants and unreacted materials. The LCST of the PNIPAM-based polymer is adjustable. It has been proved that the introduction of a hydrophilic monomer (such as AAm) into NPs leads to a higher LCST[30]. In contrast, the introduction of a hydrophobic monomer (such as TBAm) will decrease the LCST. ICG-encapsulated PNIPAM copolymer NPs were synthesized by following the above-mentioned protocols except for adding appropriate amounts of monomers, either TBAm or AAm. Because water

was used as the solvent for synthesis, 15 mol% of TBAm was found to be the maximum amount of TBAm that can be dissolved in water.

Characterization of USF contrast agents. The diameter of NPs was measured by dynamic light scattering. A 200 μL of the sample was diluted with 2.8 mL of deionized water and then measured with Nanotrac 150 (Microtrac, Inc., Nikkiso, San Diego, CA, USA). All measurements were performed in deionized water at room temperature (25°C). Transmission electron microscopy (TEM, JEOL 1200 EX, Peabody, MA) was used to determine the size and morphology of the synthesized NPs. In general, samples were prepared by drop casting an aqueous dispersion of NPs (usually at 1 mg/mL) onto a carbon-coated copper grid (FF200-Cu-50, Electron Microscopy Sciences, Hatfield, PA), followed by staining with 0.2% uranyl acetate. The components of the samples were characterized with a Fourier transform infrared (FTIR) spectrometer (Thermo Nicolet 6700, West Palm Beach, FL; see **Fig. S4**). The spectrum was taken from 4,000 to 600 cm^{-1}. A system and steps similar to the one adopted in Reference. 28 were used to characterize the optical switching properties of the USF contrast agents (see **Fig. S5**).

Setup of the USF imaging system. In **Fig. 2B**, a diode laser (MDL-III-808R) was used as the excitation light source. A band pass filter F1 (FF01-785/62-25, Semrock, New York; central wavelength: 785 nm; bandwidth: 62 nm) was used as an excitation filter to clean up any undesirable sideband components of the diode laser, which is located in the pass band of the emission filters. The shutter had a fast response time (0.5 ms). To achieve the best SNR (maximally blocking the leakage of the excitation light and maintaining a high fluorescence signal), two long pass interference filters (F2 and F5; BLP01-830R-25, Semrock, New York; edge wavelength: 846 nm) and two long pass absorptive glass filters (F3 and F4; FSR-RG830, Newport, Irvine, California, cut-on 830 nm) were adopted and positioned as shown in the figure after intensive experimental trials. The two NIR achromatic doublet lenses (AC-254-035-B, Thorlabs, New Jersey) were used to collimate the fluorescence photons for best rejecting the excitation photons by the interference filters and to focus the filtered photons onto a cooled and low-noise PMT (H7422P-20 driven by a high-voltage source C8137-02, Hamamatsu, Japan). The signal was further amplified by a low-noise current preamplifier (SR570, Stanford Research Systems, California) and acquired by a multichannel oscilloscope (DPO4102B-L, Tektronix, Oregon). A gated sinusoidal wave signal with a central frequency of 2.5 MHz was generated by the FG (33220A, Agilent, California) and was further amplified by the RF power amplifier (325LA, E&I, New York). The amplified signal was input into the NWM to drive the HIFU transducer. The HIFU transducer was focused on the small silicone tube (Instech Lab, BSIL-T031, PA). The PDG (P400, Highland, California) was used to synchronize the entire system. The HIFU transducer was mounted on a two-dimensional translation stage for both initial HIFU positioning and subsequent scanning. In the initial positioning, the HIFU transducer was moved to the position where the temperature signal from the thermocouple reached the maximum (indicating that the thermocouple junction was located on the HIFU focus). This position was considered the center of the image. A rectangular area (4.06×1.02 mm^2) was raster scanned by the HIFU transducer surrounding the center.

Ultrasound imaging. The same HIFU transducer was used to ultrasonically image the same tube in the tissue sample. A pulser/receiver (5073 PR, Olympus NDT, USA) was used for both exciting the transducer and receiving the reflected acoustic echoes. The NWM was also used for the impedance matching between the transducer and the pulser/receiver. The reflected acoustic signal was amplified by the pulser/receiver and acquired by a digitizer (NI USB 5133) interfaced to a computer. This received signal is usually called an A-line in the ultrasound imaging field and represents the tissue acoustic impendence distribution along the depth (z) direction. One A-line was acquired at each location on the x-y plane. By scanning the HIFU transducer on the x-y plane, a set of three-dimensional (x, y, and z) data was acquired. The envelope of each A-line was calculated for forming the C-mode images at different depths. To compare with the USF image, a set of two-dimensional data on the x-y plane (one of the C-mode images) was extracted by fixing the depth of z at the tube location, which formed the image shown in **Fig. 3(B)**.

Measurement of the temperature profile. A thermocouple with a small junction size of 75 μm (CHCO003, Omega Engineering, Connecticut) was put into the silicone tube to measure HIFU-induced temperature changes. The junction was fixed at the center of the scanning area. The output voltage signal from the thermocouple was amplified by an amplifier circuit consisting mainly of a high-precision operational amplifier OPA2277 and acquired by an oscilloscope (Infiniium 54830D MSO, Agilent, California). By scanning the HIFU transducer along the x direction, the temperature profile was acquired. The thermocouple signal was found linearly proportional to the temperature, which was calibrated outside the tissue sample before the test. The measured peak temperature at the HIFU focus was found to be around 45°C.

Measurement of the profile of the diffuse fluorescence light. To acquire the profile of the diffused fluorescence light, as shown in **Fig. 3C**, the sample was scanned along the x direction while all the other components remained fixed. Although the HIFU remained off and the temperature was kept at room temperature (<LCST), the USF contrast agents still emitted some fluorescence when the laser was on because the USF contrast agents are not 100% off even in the off state. To avoid the effect of the excitation light on the results due to the emission filter leakage, a background scan was conducted by filling the tube with water, and the data was subtracted from the result acquired from the tube filled with the contrast agents.

1. Andresen, V. *et al.* Infrared multiphoton microscopy: subcellular-resolved deep tissue imaging. *Curr. Opin. Biotechnol.* **20**, 54–62, doi:10.1016/j.copbio.2009.02.008 (2009).
2. Helmchen, F. & Denk, W. Deep tissue two-photon microscopy. *Nat Methods* **2**, 932–940, doi:10.1038/nmeth818 (2005).
3. Cai, W. & Chen, X. Multimodality molecular imaging of tumor angiogenesis. *J Nucl Med* **49 Suppl 2**, 113S–128S, doi:10.2967/jnumed.107.045922 (2008).
4. McDonald, D. M. & Choyke, P. L. Imaging of angiogenesis: from microscope to clinic. *Nature Medicine* **9**, 713–725, doi:10.1038/nm0603-713 (2003).
5. Corlu, A. *et al.* Three-dimensional in vivo fluorescence diffuse optical tomography of breast cancer in humans. *Opt. Express* **15**, 6696–6716, doi:10.1364/OE.15.006696 (2007).
6. Culver, J., Akers, W. & Achilefu, S. Multimodality molecular imaging with combined optical and SPECT/PET modalities. *Journal of Nuclear Medicine* **49**, 169–172, doi:10.2967/jnumed.107.043331 (2008).
7. Wang, L. V. Multiscale photoacoustic microscopy and computed tomography. *Nature Photonics* **3**, 503–509, doi:10.1038/nphoton.2009.157 (2009).
8. Yuan, B. & Zhu, Q. Separately reconstructing the structural and functional parameters of a fluorescent inclusion embedded in a turbid medium. *Optics Express* **14**, 7172–7187, doi:10.1364/OE.14.007172 (2006).
9. Razansky, D. *et al.* Multispectral opto-acoustic tomography of deep-seated fluorescent proteins in vivo. *Nature Photonics* **3**, 412–417, doi:10.1038/Nphoton.2009.98 (2009).
10. Yuan, B., Liu, Y., Mehl, P. & Vignola, J. Microbubble-enhanced ultrasound-modulated fluorescence in a turbid medium. *Applied Physics Letters* **95**, 181113–181113, doi:10.1063/1.3262959 (2009).
11. Kobayashi, M., Mizumoto, T., Shibuya, Y., Enomoto, M. & Takeda, M. Fluorescence tomography in turbid media based on acousto-optic modulation imaging. *Applied Physics Letters* **89**, 181102, doi:10.1063/1.2364600 (2006).
12. Huynh, N. T., Hayes-Gill, B. R., Zhang, F. & Morgan, S. P. Ultrasound modulated imaging of luminescence generated within a scattering medium. *J. Biomed. Opt.* **18**, doi:10.1117/1.jbo.18.2.020505 (2013).
13. Lin, Y., Bolisay, L., Ghijsen, M., Kwong, T. C. & Gulsen, G. Temperature-modulated fluorescence tomography in a turbid media. *Applied Physics Letters* **100**, 73702–737024, doi:10.1063/1.3681378 (2012).
14. Lin, Y., Kwong, T. C., Bolisay, L. & Gulsen, G. Temperature-modulated fluorescence tomography based on both concentration and lifetime contrast. *J. Biomed. Opt.* **17**, 056007–056001, doi:10.1117/1.jbo.17.5.056007 (2012).
15. Yuan, B., Uchiyama, S., Liu, Y. K. N. T. & Alexandrakis, G. High-resolution imaging in a deep turbid medium based on an ultrasound-switchable fluorescence technique. *Applied Physics Letters* **101**, 033703, doi:10.1063/1.4737211 (2012).
16. Xu, X. A., Liu, H. L. & Wang, L. V. Time-reversed ultrasonically encoded optical focusing into scattering media. *Nature Photonics* **5**, 154–157, doi:10.1038/Nphoton.2010.306 (2011).
17. Wang, Y. M., Judkewitz, B., DiMarzio, C. A. & Yang, C. H. Deep-tissue focal fluorescence imaging with digitally time-reversed ultrasound-encoded light. *Nat Commun* **3**, doi:10.1038/Ncomms1925 (2012).
18. Si, K., Fiolka, R. & Cui, M. Fluorescence imaging beyond the ballistic regime by ultrasound-pulse-guided digital phase conjugation. *Nature Photonics* **6**, 657–661, doi:10.1038/nphoton.2012.205 (2012).
19. Judkewitz, B., Wang, Y. M., Horstmeyer, R., Mathy, A. & Yang, C. Speckle-scale focusing in the diffusive regime with time reversal of variance-encoded light (TROVE). *Nature Photonics* **7**, 300–305, doi:10.1038/nphoton.2013.31 (2013).
20. Si, K., Fiolka, R. & Cui, M. Breaking the spatial resolution barrier via iterative sound-light interaction in deep tissue microscopy. *Scientific Reports* **2**, doi:10.1038/srep00748 (2012).
21. Konecky, S. D. & Tromberg, B. J. IMAGING Focusing light in scattering media. *Nature Photonics* **5**, 135–+, doi:DOI 10.1038/nphoton.2011.19 (2011).
22. Weissleder, R. & Ntziachristos, V. Shedding light onto live molecular targets. *Nature Medicine* **9**, 123–128, doi:10.1038/Nm0103-123 (2003).
23. Chen, Y. & Li, X. Near-Infrared Fluorescent Nanocapsules with Reversible Response to Thermal/pH Modulation for Optical Imaging. *Biomacromolecules* **12**, 4367–4372, doi:10.1021/bm201350d (2011).
24. Gota, C., Uchiyama, S., Yoshihara, T., Tobita, S. & Ohwada, T. Temperature-Dependent Fluorescence Lifetime of a Fluorescent Polymeric Thermometer, Poly(N-isopropylacrylamide), Labeled by Polarity and Hydrogen Bonding Sensitive 4-Sulfamoyl-7-aminobenzofurazan. *The Journal of Physical Chemistry B* **112**, 2829–2836, doi:10.1021/jp709810g (2008).
25. Wang, D. P., Miyamoto, R., Shiraishi, Y. & Hirai, T. BODIPY-Conjugated Thermoresponsive Copolymer as a Fluorescent Thermometer Based on Polymer Microviscosity. *Langmuir* **25**, 13176–13182, doi:10.1021/La901860x (2009).
26. Yuan, B. H., Chen, N. G. & Zhu, Q. Emission and absorption properties of indocyanine green in Intralipid solution. *J. Biomed. Opt.* **9**, 497–503, doi:Doi 10.1117/1.1695411 (2004).
27. Yuan, B. H., Pei, Y. B. & Kandukuri, J. Breaking the acoustic diffraction limit via nonlinear effect and thermal confinement for potential deep-tissue high-resolution imaging. *Applied Physics Letters* **102**, doi:Doi 10.1063/1.4792736 (2013).

28. Cheng, B. *et al*. Development of Ultrasound-Switchable Fluorescence Imaging Contrast Agents Based on Thermosensitive Polymers and Nanoparticles. *IEEE Journal of Selected Topics in Quantum Electronics* **20**, 6801214, doi:10.1109/JSTQE.2013.2280997 (2014).
29. Yang, Q., Xu, X., Lai, P., Xu, D. & Wang, L. V. Time-reversed ultrasonically encoded optical focusing using two ultrasonic transducers for improved ultrasonic axial resolution. *J. Biomed. Opt.* **18**, 110502–110502, doi:10.1117/1.jbo.18.11.110502 (2013).
30. Rahimi, M. *et al*. Synthesis and Characterization of Thermo-Sensitive Nanoparticles for Drug Delivery Applications. *J Biomed Nanotechnol* **4**, 482–490, doi:10.1166/Jbn.2008.014 (2008).

Acknowledgments

This work was supported in part by funding from the NIH/NIBIB 7R15EB012312-02 (Yuan), the CPRIT RP120052 (Yuan) and the NSF CBET-1253199 (Yuan). The authors are grateful to Drs. Hanli Liu and Yi Hong for sharing lab equipment and to Ms Jyothi U. Menon for TEM measurement.

Author Contributions

B.Y. designed the experiment. Y.P. implemented the imaging experiment and analyzed the image data. Z.X. and K.N. designed the synthesis protocol of the USF contrast agents. M.-Y.W. and B.C. synthesized the contrast agents and M.-Y.W., B.C. and Y.L. characterized the contrast agents. B.Y., M.-Y.W. and Y.P. prepared the manuscript. All authors reviewed the manuscript.

Additional information

Supplementary information accompanies this paper at http://www.nature.com/scientificreports

Competing financial interests: The authors declare no competing financial interests.

How to cite this article: Pei, Y.B. *et al*. High resolution imaging beyond the acoustic diffraction limit in deep tissue *via* ultrasound-switchable NIR fluorescence. *Sci. Rep.* **4**, 4690; DOI:10.1038/srep04690 (2014).